International Journal of Heat and Technology
Vol. 43, No. 6, December, 2025, pp. 2350-2358
Journal homepage: http://iieta.org/journals/ijht

Thermal–Solutal Dynamics Between Rotating Disks in Bio-Stabilised ZnO Hybrid Nanofluids: Coupled FEM and Neural Network Analysis

Kotike Jyothi[1], Vikram Madithan[2], Ganapati Ramavat[3], Harinadh Vemanaboina[4], M.V.V. Prasad Kantipudi[5*]

[1] Department of Humanities and Basic Sciences, G Pulla Reddy Engineering College, Kurnool, 518007, India
[2] Department of Computer Science Engineering, Sri Venkateswara College of Engineering, Tirupati 517507, India
[3] Department of Mechanical Engineering, Anurag Engineering College (Autonomous) Kodad, Telangana 508206, India
[4] Department of Mechanical Engineering, VEMU Institute of Technology, Chittoor 517112, India
[5] Symbiosis Institute of Technology, Symbiosis International (Deemed University), Pune 412115, India

Corresponding Author Email: mvvprasad.kantipudi@gmail.com

https://doi.org/10.18280/ijht.430632

Received: 10 October 2025
Revised: 18 December 2025
Accepted: 26 December 2025
Available online: 31 December 2025

Keywords:
Aloe vera stabilized ZnO nanoparticles, MHD effects, upper and lower disk, finite element method (fem), Levenberg–Marquardt neural network

ABSTRACT

The paper is based on the demand for sustainable and high-performance thermal fluids through the analysis of the properties of heat and mass transfer of a green hybrid nanofluid, Aloe vera extract-stabilised ZnO nanoparticles in water, operating between two coaxial parallel rotating disks. Those two nonlinear governing equations coupled with magnetohydrodynamic terms and thermal radiation ones are solved numerically by the Galerkin-based finite element method (FEM) with the use of Mathematica. The modified mixture models are developed to take into consideration the effects of bio-surfactant stabilisation on the effective thermophysical properties. To further elaborate on the numerical simulations, a feedforward artificial neural network that has been trained on the Levenberg-Marquardt algorithm in MATLAB is created to extrapolate the wall shear stress, Nusselt number, and Sherwood number to a variety of nanoparticle concentrations, magnetic field intensities, and disk rotation rates. The findings indicate that there is strong transport asymmetry between the disks: The rise in angular velocity substantially improves the heat transfer and inhibits the solutal boundary layer in the upper disk and the mass transfer in the lower disk is stronger in the lower disk as a result of the momentum confinement. Enhancement of heat transfer is mostly conditioned by the nanoparticle loading in the upper disk, but the mass transfer enhancement is prevalent in the lower disk. The ANN surrogate has strong predictive capability, well able to capture disk-specific transport behaviour, and can be used to provide a parametric evaluation quickly. These results demonstrate the possibility of Aloe vera-ZnO/water nanofluids as a thermal working fluid that is environmentally friendly and can be used in rotating machinery, bioreactors, and disk-based heat and mass transfer.

1. INTRODUCTION

Nanotechnology is becoming increasingly popular, allowing the creation of hybrid nano-fluid suspensions of nanoparticles in base fluids that exhibit superior characteristics. Bio-hybrid nanofluids, such as those derived from Aloe vera extract, offer the advantages of being eco-friendly and exhibiting improved thermal conductivity. Hybrid nanofluids are examined for their heat transfer properties in various systems, and their transport properties are controlled accurately. They improve the convective heat transfer and are environmentally friendly. A hybrid nanofluid study involves the incorporation of various nanoparticles into base fluids to promote the transfer of heat and mass within the engineering systems. Such nanofluids exhibit improved thermal conductivity and adjustable properties. Aloe vera stabilized ZnO/water. The bio-hybrid nanofluids, such as those derived from Aloe vera, offer a new alternative material for thermal management. Bio-hybrid nanofluids have applications in high-performance systems that require adequate heat and mass transfer.

An example of rotating disk systems is the two-disk system, which is utilised in engineering processes such as turbines, reactors, and pumps, where centrifugal forces, viscous dissipation, and thermal gradients significantly influence the complex transport behaviour. Nevertheless, the investigations in literature focus more on traditional hybrid or ternary nanofluids, excluding bio-based stabilization or FEM-ANN predictive models in monolithic rotating disk setups [1-3]. FEM is effective in solving the governing nonlinear PDEs in such geometries, and trained ANNs using LM offer fast, accurate surrogate modelling of important outputs such as Nusselt and Sherwood numbers [4, 5], which are useful to study parameters of interest efficiently.

The positive impact of hybrid nanofluids in rotating disk systems is supported in recent studies. Afzal et al. [1]

optimized the entropy generation of hybrid nanofluid flow over disks, enhancing thermal performance and controlling the boundary layer. The study by Noreen et al. [2] focuses on ternary hybrids, where the thermal radiation and Cattaneo-Christov flux are of interest, specifically examining the synergy between nanoparticles. The use of AI and numerical methods is also on the rise. Nasir et al. [4] compared ANNs with the prediction of the heat transport in magnetized porous cavities. Still, Ramzan et al. [5] and Alqahtani et al. [6] used FEM to simulate hybrid flows (over rotating surfaces). Disks were experimented on and had a shrinking diameter; heat transfer was dependent on rotation and magnetism [3]. However, these papers only use numerical simulations or stand-alone AI models but do not combine ANN surrogates and high-fidelity FEM solvers to model asymmetric heat and mass transfer in two-disk systems. Recently, tetra-hybrid nanofluids were introduced by Sakkaravarthi et al. [7], which enhance entropy-based thermal transport. LM-ANNs can model the nonlinear effects of parameters such as the volume fraction of nanoparticles, slip, magnetic fields, and heat sources [8, 9]. They are helpful in rapid surrogate modeling, which substitutes expensive FEM executions. In contrast to the current research, those studies do not involve ANN-Levenberg-Marquardt training in combination with FEM-generated data to provide intelligent approximations of nonlinear ODEs developed on the basis of coupled PDEs. They can be used in solar collectors, MHD wavy enclosures, and more complicated nanofluid flows [10, 11]. LM-ANNs are fast, convergent, accurate, and robust in the analysis of asymmetric heat/mass transfer.

Recent publications emphasise that Aloe vera–ZnO/water nanofluids are sustainable and high-performing thermal systems, as they exhibit higher conductivity rates; nevertheless, the asymmetric transport behavior of bio-based Aloe vera-ZnO/water nanofluids in upper-lower rotating disk systems has not been accurately measured, and or predicted using machine learning-based numerical models. stability, and green synthesis [12, 13]. Thermophysical correlations of ZnO and Al_2O_3 nanofluids are reliable, which justifies the proper modelling [14]. FEM simulations can model complex hybrid nanofluid behaviour in MHD, Joule heating, and chemical effects [15-17]. Rotating disk studies indicate asymmetric transfer, which is essential in convective transfer [18], supporting the importance of Aloe vera ZnO/water nanofluids in the use of the two disks.

Although there has been an improvement in hybrid nanofluid studies, gaps remain in bio-based systems, in double-disk configurations are particularly desirable. Synthesized nanoparticles, single disks, or traditional fluids have been studied in most of the literature on MHD, radiation, and slip effects [1, 2, 18-20]. Specifically, the interactive effect of the magnetic field, thermal radiation, and slip boundary conditions on Aloe vera-ZnO/water nanofluids in dual rotating disks is not discussed before. Besides, there is no literature on FEM-LM-ANN hybrid modeling approaches to such green nanofluids are not well studied, especially in terms of upper-lower disk asymmetries. In order to fill these gaps, the current research provides the following new contributions:

(i) A flow of Aloe vera-ZnO/water nanofluid between a pair of coaxial rotating disks was modelled by the Galerkin-based FEM using the Mathematica software;

(ii) The quantitative analysis of the upper-lower disk inequity of heat and mass transfer when magnetic, radiation, and slip forces are present; and

(iii) Building an ANN-Levenberg-Marquardt surrogate model, which is able to predict Nusselt number, Sherwood number, and wall shear stress under the influence of parametric variations accurately.

This bilateral FEMANN model allows a smart representation of nonlinear transport processes with substantial computational cost reduction, which provides a unique improvement over the current literature.

Although hybrid and ternary nanofluids have a considerable amount of literature, the literature on the topic of Aloe vera ZnO/water nanofluid is very scarce. The available literature mainly highlights traditional metal, or metal-oxide nanofluids, and highlights general thermal enhancement, and the synergistic effect of magnetic field, thermal radiation, and slip boundary condition on Aloe vera-ZnO nanofluids has not been studied thoroughly, especially in rotating disk systems. Furthermore, advanced predictive frameworks or numerical models have not been used to report the presence of thermal-hydrodynamic asymmetries and the coupled nature of heat-mass transfer of this bio-stabilized nanofluid. The role of the current study in filling this gap is an in-depth FEM-based analysis with the addition of ANN–Levenberg-Marquardt modeling, which will provide new knowledge regarding the transport characteristics and the potential practical potential of Aloe vera-ZnO/water nanofluids in thermal systems with environmental friendliness.

2. MATHEMATICAL FORMULATION

This research analyses the behaviour of a fluid containing Aloe Vera-ZnO/water nanofluids as it moves in space between two rotating disks, as depicted in Figure 1. The fluid is electrically conductive, and the study focuses on its steady, symmetrical flow and the transfer of heat, while also considering the effects of viscosity and an applied magnetic field. The system consists of a lower disk positioned at $z = 0$ and an upper disk fixed at a height $z = h$. Both disks are porous, can stretch, and rotate continuously, but they do so at independent speeds. They also stretch radially and axially at different rates. Thermally, the disk surfaces follow convective boundary conditions, with the bottom and top disks maintained at distinct, constant temperatures. A uniform magnetic field is directed perpendicular to the disks, along the z-axis. The governing equations for mass, momentum, and energy conservation are formulated for this configuration using cylindrical coordinates. These equations account for the heat transfer contributed by thermal radiation. The physical properties of the base fluid (water) and the Aloe Vera-ZnO are provided in Table 1.

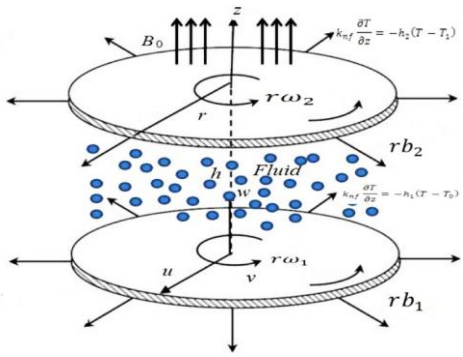

Figure 1. Geometrical representation

Table 1. Thermophysical properties of nanofluids [12, 14]

Fluid	ρ (kg/m³)	Cp (J/kg·K)	K (W/m·K)
Water	997.1	4179	0.613
Aloe vera extract Nanoparticles	980–1020	3900–4200	0.25–0.35
ZnO Nanoparticles	5600–5700	500–550	25–60

$$\frac{\partial u_1}{\partial r}+\frac{u_1}{r}+\frac{\partial w_1}{\partial z}=0 \tag{1}$$

$$u_1\frac{\partial u_1}{\partial r}-\frac{v_1^2}{r}+w_1\frac{\partial u_1}{\partial z}=-\frac{1}{\rho_{nf}}\frac{\partial p}{\partial r}+\frac{\mu_{nf}}{\rho_{nf}}\left(\frac{\partial^2 u_1}{\partial r^2}+\frac{1}{r}\frac{\partial u_1}{\partial r}-\frac{u_1}{r^2}+\frac{\partial^2 u_1}{\partial z^2}\right)-\frac{\mu_{nf}}{\rho_{nf}}\frac{1}{K}u_1-\frac{\sigma_{nf}}{\rho_{nf}}B_0{}^2u_1 \tag{2}$$

$$u_1\frac{\partial v}{\partial r}+\frac{u_1v_1}{r}+w_1\frac{\partial v_1}{\partial z}=\frac{\mu_{nf}}{\rho_{nf}}\left(\frac{\partial^2 v_1}{\partial r^2}+\frac{1}{r}\frac{\partial v_1}{\partial r}-\frac{v_1}{r^2}+\frac{\partial^2 v_1}{\partial z^2}\right)-\frac{\mu_{nf}}{\rho_{nf}}\frac{1}{K}v_1-\frac{\sigma_{nf}}{\rho_{nf}}B_0{}^2v_1 \tag{3}$$

$$u_1\frac{\partial w_1}{\partial r}+w_1\frac{\partial w_1}{\partial z}=-\frac{1}{\rho_{nf}}\frac{\partial p}{\partial r}\frac{\mu_{nf}}{\rho_{nf}}\left(\frac{\partial^2 w_1}{\partial r^2}+\frac{1}{r}\frac{\partial w_1}{\partial r}+\frac{\partial^2 w_1}{\partial z^2}\right)-\frac{\mu_{nf}}{\rho_{nf}}\frac{1}{K}w_1 \tag{4}$$

$$u_1\frac{\partial T_1}{\partial r}+w_1\frac{\partial T_1}{\partial z}=\frac{k_{nf}}{(\rho c_p)_{nf}}\left(\frac{\partial^2 T_1}{\partial r^2}+\frac{1}{r}\frac{\partial T_1}{\partial r}+\frac{\partial^2 T_1}{\partial z^2}\right)-\frac{1}{(\rho c_p)_{nf}}\frac{\partial q_r}{\partial z} \tag{5}$$

$$u_1\frac{\partial C}{\partial r}+w_1\frac{\partial c}{\partial z}=D_B\frac{\partial^2 C}{\partial z^2}-K_r(c-c_\infty) \tag{6}$$

The associated boundary conditions are:

$$u_1=rb_1\ \ ,v_1=r\omega_1,\ \ w_1=0,\ \ k_{nf}\frac{\partial T}{\partial z}=-h_1(T_0-T_1)\ \text{at}\ z=0 \tag{7}$$

$$u_1=rb_2\ \ ,\ v_1=r\omega_2,\ w_1=0,\ k_{nf}\frac{\partial T}{\partial z}=-h_2(T_1-T_2)\ at\ z=h \tag{8}$$

The stream function ψ can be defined as follows,

$$u_1=\frac{\partial \psi}{\partial y},\ v_1=-\frac{\partial \psi}{\partial x} \tag{9}$$

To simplify the governing equations for analysis, the following dimensionless variables are introduced.

$$\begin{aligned} &u_1=r\omega_1\, f'(\eta),\ v_1=r\,\omega_1 g,\ w=-\sqrt{2\,\omega_1\,\nu_f}\,f(\eta),\\ &\eta=\frac{z}{h},\ \theta(\eta)=\frac{T_0-T_1}{T_1-T_2},\ p=\rho_f\nu_f\omega_1\left(P(\eta)+\frac{1}{2}\,\frac{r^2}{h^2}\,\varepsilon\right). \end{aligned} \tag{10}$$

The physical properties of the nanofluid, including its dynamic viscosity and density, are defined in terms of the base fluid and nanoparticle constituents. Similarly, its thermal characteristics, including thermal diffusivity and conductivity, have been established. The model also incorporates the heat capacity and electrical conductivity of the fundamental fluid.

$$A_1=\frac{1}{(1-(\phi_1+\phi_2))^{2.5}}\ ,\ A_2=[(1-(\phi_1+\phi_2)+\phi_1(\frac{\rho_{s1}}{\rho_f})+\phi_2(\frac{\rho_{s2}}{\rho_f})],$$
$$A_3=[(1-(\phi_1+\phi_2)+\phi_1(\frac{(\rho c_p)_{s1}}{(\rho c_p)_f})+\phi_2(\frac{(\rho c_p)_{s2}}{(\rho c_p)_f})],\ A_4=\frac{k_{hnf}}{k_f}.$$

μ_{hnf}, ρ_{hnf}, α_{hnf}, k_{hnf}, $(\rho c_p)_{hnf}$, σ_{hnf} of the hybrid nano fluid, ν_f of the base fluid are characterized by the following expressions:

$$\mu_{hnf}=\frac{\mu_f}{(1-(\phi_1+\phi_2))^{2.5}},\ \rho_{hnf}=(1-(\phi_1+\phi_2))\,\rho_f+\phi_1(\rho)_{s1}+\phi_2(\rho)_{s2} \tag{11}$$

$$(\rho c_p)_{hnf}=(1-(\phi_1+\phi_2))\,\rho c_{p_f}+\phi_1(\rho c_p)_{s1}+\phi_2(\rho c_p)_{s2}$$
$$k_{hnf}=k^*_{nf}(\frac{k_{s2}+2k_{nf}-2\phi_2(k_{nf}-k_{s2})}{k_{s2}+2k_{nf}+\phi_2(k_{nf}-k_{s2})})$$
$$k_{nf}=k^*_f(\frac{k_{s1}+2k_f-2\phi_2(k_f-k_{s1})}{k_{s1}+2k_f+\phi_2(k_f-k_{s1})})$$

The radiative heat flux is modeled via the Rosseland approximation, as follows:

$$q_r=-\frac{4\sigma^*}{3K^*}\frac{\partial T^4}{\partial z} \tag{12}$$

Through the use of Eqs. (9)-(11), the original governing equations, comprising the nonlinear partial differential Eqs. (1) through (5) and the boundary conditions (7) and (8), are reduced to a system of ordinary differential equations.

$$f'''-\frac{A_1}{2}\,\mathrm{Re}\left[(f')^2-2f\,f''-g^2\right]-k_1f'-\frac{A_1}{A_2}.Mf'-\frac{A_1}{A_2}\varepsilon=0 \tag{13}$$

$$g''+A_1\mathrm{Re}[2fg'-2f'g]-k_1\,g-\frac{A_1}{A_2}.M\,g=0 \tag{14}$$

$$P'+4\,A_2\,Re\,ff'+2\,\frac{A_2}{A_1}\,f''=0 \tag{15}$$

$$(1+R)\theta''+2\,Re.\mathrm{Pr}.\,A_3\,A_4\,f\theta'=0 \tag{16}$$

$$\phi''-\mathrm{Sc}\,\mathrm{Cr}\,\phi+Nt/Nb\,\theta''=0 \tag{17}$$

The application of the similarity transformations yields the following boundary conditions:

$$\begin{aligned} &\eta=0, f=0, f'=B_1, g=1, \theta'=-\left(\frac{1}{A_4}\right)B_4(1-\theta)\\ &\eta=1, f'=B_2, g=B_3, \theta'=-\left(\frac{1}{A_4}\right)B_5(1-\theta). \end{aligned} \tag{18}$$

The fundamental physical parameters investigated in the present analysis include the skin friction coefficients and Nusselt numbers at both the lower and upper disks. These quantities are mathematically expressed as:

$$C_1=\frac{\tau_{rz}}{\rho_f(r\omega_1)^2},\ C_2=\frac{\tau_{\theta z}}{\rho_f(r\omega_2)^2},\ \mathrm{Nu}_{x1}=\frac{hq_w}{k_f(T_0-T_1)},\ \mathrm{Nu}_{x2}=\frac{hq_w}{k_f(T_0-T_1)},$$
$$C_1=\frac{\tau_w|_{z=0}}{\rho_f(r\omega_1)^2}=\frac{\left(\left(f''(0)\right)^2+\left(g'(0)\right)^2\right)^{1/2}}{(1-\varphi)^{2.5}\mathrm{Re}_r},$$
$$C_2=\frac{\tau_w|_{z=h}}{\rho_f(r\omega_1)^2}=\frac{\left(\left(f''(1)\right)^2+\left(g'(1)\right)^2\right)^{1/2}}{(1-\varphi)^{2.5}\mathrm{Re}_r},$$
$$\mathrm{Nu}_1=-(A_4+R)\theta'(0)\ \ ,\ \mathrm{Nu}_2=-(A_4+R)\theta'(1)$$

where, $\tau_w=(\tau^2_{rz}+\tau^2_{\theta z})^{1/2}$ is the total shear stress.

3. NUMERICAL METHOD

Due to the high nonlinearity of the ordinary differential Eqs. (15)–(18), obtaining an analytical solution is impractical. Hence, the finite element method (FEM) [21-27] has been adopted to tackle these equations. The general computational procedure of FEM is summarized below.

3.1 Finite element method

To solve the problem of the non-linear ordinary differential Eqs. (13)–(17) with boundary conditions (18), we suppose in the beginning.

$$\frac{df}{d\eta}=h \tag{19}$$

The Eqs. (11) to (13) then reduces to:

$$h''-\frac{A_1}{2}\mathrm{Re}\left[h^2-2fh'-g^2\right]-k_1\,h-\frac{A_1}{A_2}Mh=0 \tag{20}$$

$$g''+A_1\mathrm{Re}[2fg'-2hg]-k_1 g-\frac{A_1}{A_2}Mg=0 \tag{21}$$

$$(1+R)\theta''+2\,\mathrm{Re}\,\mathrm{Pr}\,A_3\,A_4\,f\,\theta'=0 \tag{22}$$

$$\emptyset''-\mathrm{Sc}\,\mathrm{Cr}\,\emptyset+\mathrm{Nt}/\mathrm{Nb}\,\theta''=0 \tag{23}$$

The boundary conditions take the form $\eta=0, f=0, h=B_1, g=1, \theta'=-\left(\frac{1}{A_4}\right)B_4(1-\theta)$.

$$\eta=1, h=B_2, g=B_3, \theta'=-\left(\frac{1}{A_4}\right)B_5(1-\theta). \tag{24}$$

In order to determine the correctness and consistency of the suggested finite element model, the current FEM solutions are compared to the benchmark solutions obtained previously in the literature regarding the same rotating disk and MHD nanofluid flow configurations. At the end limits of negligible magnetic field, radiation, and nanoparticle loading, the calculated velocity and temperature profiles agree with the classical findings of Newtonian fluids rooted in rotating disks very well. Moreover, the trends derived by the prediction of Nusselt and Sherwood numbers at different rotational and magnetic parameters are in line with previous numerical studies done on hybrid nanofluids in rotating geometries. The fact that the current FEM solutions are in close agreement with the benchmark results provided above confirms that the resulting Galerkin-based FEM implementation recapitulates the underlying transport physics. This justifies the adoption of the current numerical model in the analysis of the more complicated system, the Aloe vera-ZnO/water nanofluid system in this research.

4. RESULTS AND DISCUSSIONS

The findings reveal the existence of specific transport characteristics within the Aloe vera-ZnO/water hybrid nanofluid system, as observed between two coaxial rotational disks. Figures 2 and 3 indicate that as the volume fraction of primary nanoparticles, ϕ1, increases, both velocity and temperature profiles become more intense, with the upper disk demonstrating better thermal and momentum diffusion due to its higher angular velocity. Similarly, Figures 4 and 5 show that the secondary volume fraction, ϕ2, enhances the flow and heat transfer, demonstrating the synergistic effect of the dual nanoparticles. The strength of the magnetic field M, as indicated in Figure 6, inhibits velocity on both disks due to Lorentz drag, with the lower disk experiencing this effect more significantly because of the confined momentum field. The radiation effects (Figures 7 and 8) enhance the temperature profiles, especially around the upper disk, although they slightly decrease the velocity due to the dispersion of thermal energy. The Schmidt number Sc, as studied in Figures 9 and 10, affects solutal transport; the larger the Schmidt number, the less concentrated the concentration boundary layer and the lower the temperature, indicating faster mass diffusion. The intensity of the chemical reaction Cr, represented in Figures 11-13, decreases the velocity, temperature, and concentration profiles, with the bottom disk exhibiting steeper falls due to reactive depletion that is more severe. The asymmetry between the upper and lower disks is evident in all parametric variations, with thermal enhancement effects prevailing toward the upper disk and solutal effects being dominant toward the lower disk.

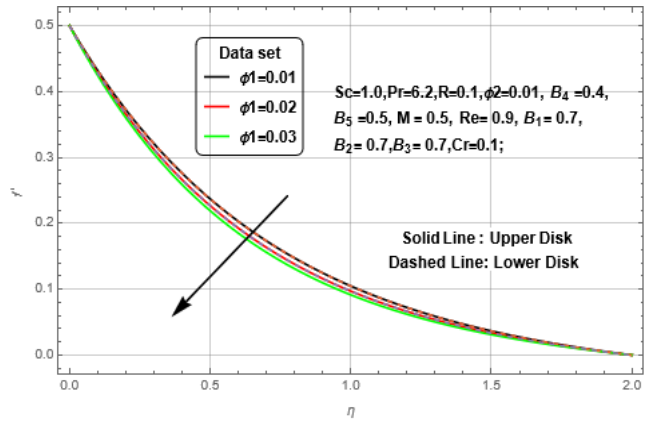

Figure 2. f′(η) vs η effect of volume fraction parameter ϕ1

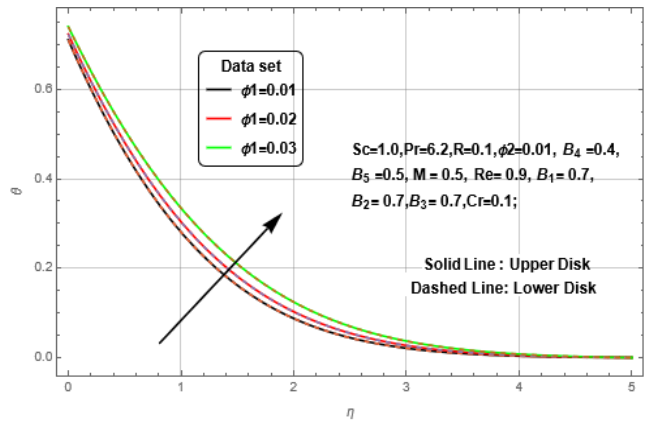

Figure 3. θ(η) vs η effect of volume fraction parameter ϕ1

According to the data in Table 2, both the skin friction coefficient (Cfx) and Nusselt number (Nux) are highly responsive to variations in the nanoparticle volume fraction (ϕ_1), magnetic field strength (M), radiation parameter (R), Schmidt number (Sc), and chemical reaction rate (Cr) for the Aloe vera–ZnO/water hybrid nanofluid flow between rotating disks. The increase of ϕ1 increases the Cfx through the rise in the momentum diffusion and decreases Nux, which is a sign of thermal saturation; the increase in ϕ2 decreases both Cfx and Nux, which are signs of the addition of viscous resistance. The magnetic intensification (M) increases Cfx and suppresses Nux, as is consistent with the Lorentz damping. Effects of radiation (R) increase Cfx at the top disk but decrease Cfx at

the bottom, and Nux decreases everywhere because of thermal dispersion. The increase in Sc causes a slight decrease in Cfx but a sudden increase in Nux, resulting in increased thermal transport with a reduced mass diffusivity. The parameter Cr of the chemical reaction has a strong suppressing effect on Cfx and Nux, particularly in the lower part of the disk, due to the depletion of reactive energy and momentum. In all cases, the upper disk is characterized by greater Cfx and Nux, indicating asymmetric transport behavior due to dissimilar rotation and a constrained boundary.

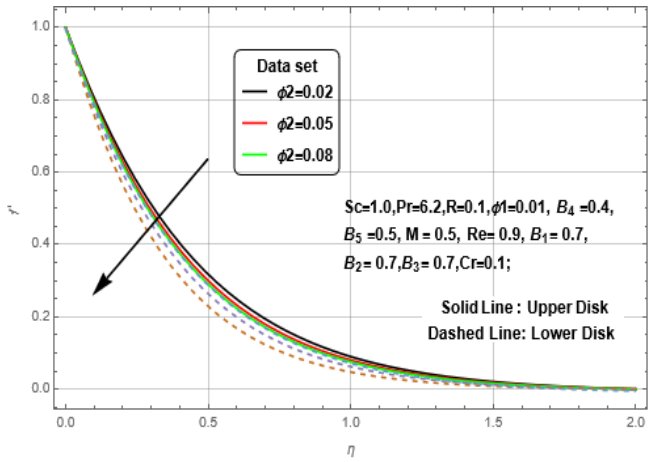

Figure 4. f′(η) vs η effect of volume fraction parameter ϕ2

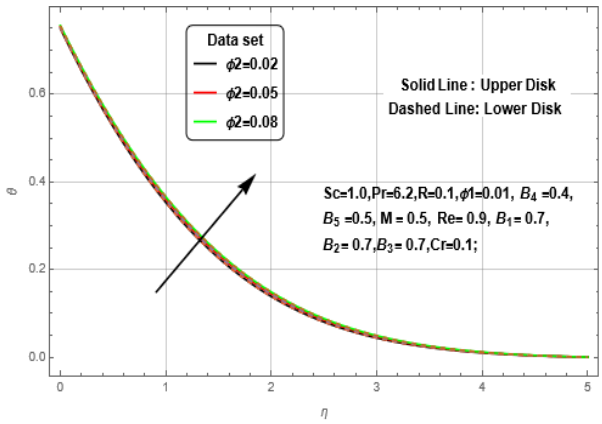

Figure 5. θ(η) vs η effect of volume fraction parameter ϕ2

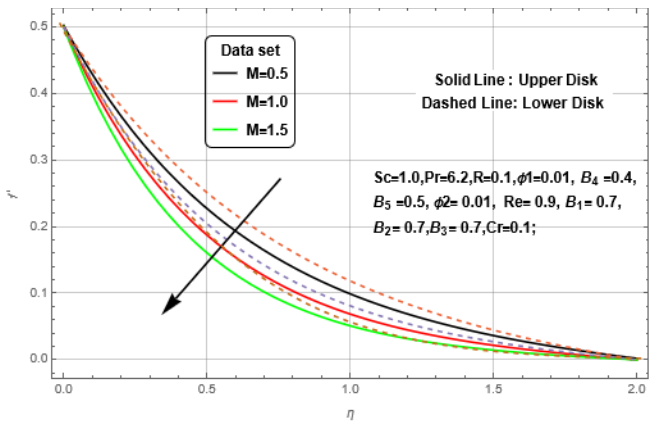

Figure 6. f′(η) vs η effect of magnetic parameter M

Figures 14-17 present the performance analysis of the trained Levenberg-Marquardt artificial neural network, providing information on model accuracy, convergence, and generalization using training, validation, and test datasets. In contrast, Figure 18 presents the neural network architecture. Figure 14 illustrates the trajectory of the mean squared error (MSE) after 7 epochs. The optimal result, achieved by using the model to validate the data, was obtained at epoch 1 (MSE = 1.227), indicating that the model converged very quickly and did not overfit. This is further supported by Figure 15, which shows a progressively declining gradient (down to 2.4497e-08) and μ value (dropping to 1e-10) at epoch 7, confirming that the network has reached a steady minimum. The number of check counts of the validation, 6, indicates that the model was generalized without overtraining.

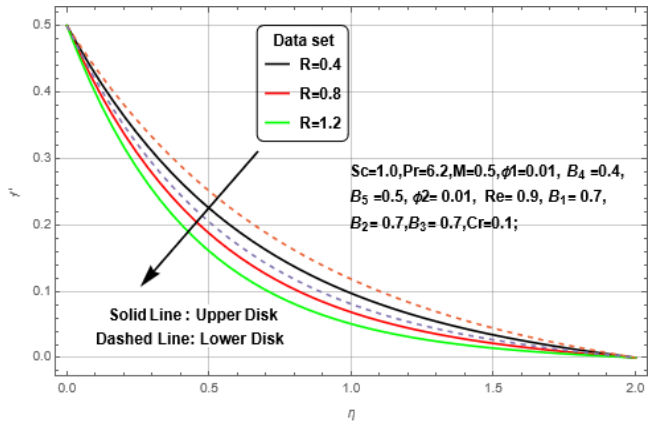

Figure 7. f′(η) vs η effect of radiation parameter R

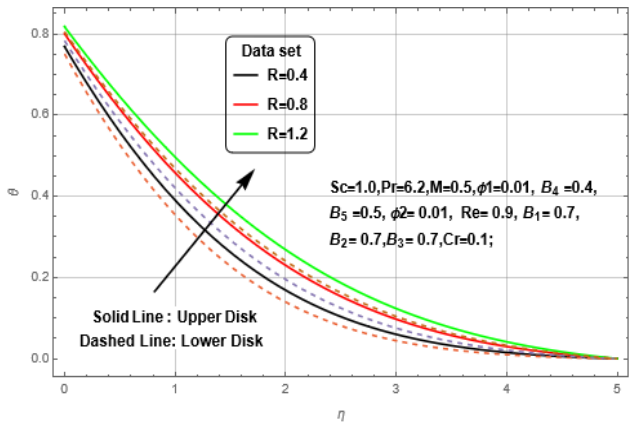

Figure 8. θ(η) vs η effect of radiation parameter R

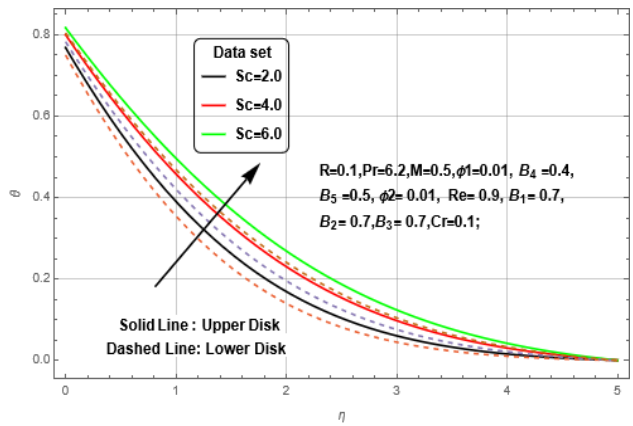

Figure 9. θ(η) vs η effect of Sc

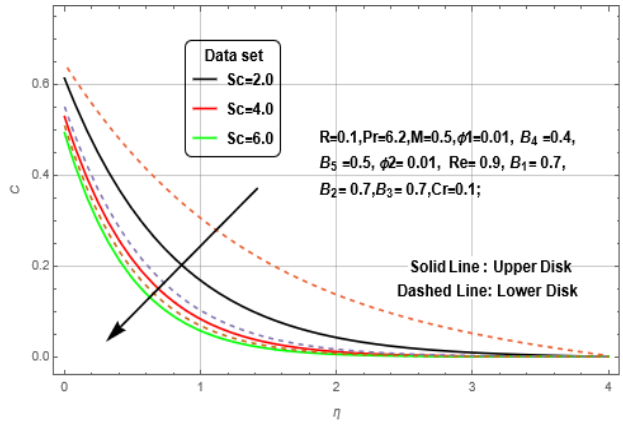

Figure 10. C(η) vs η effect of Sc

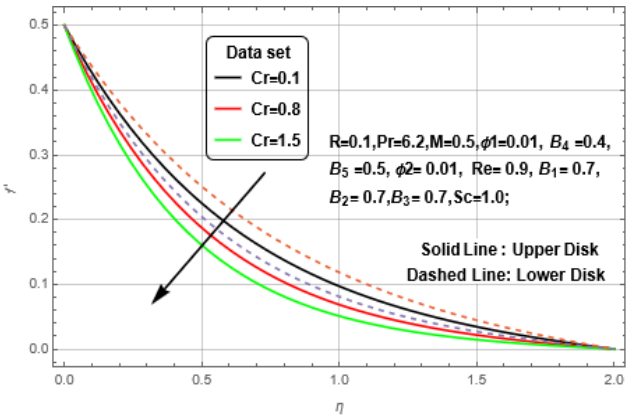

Figure 11. f′(η) vs η effect of Cr

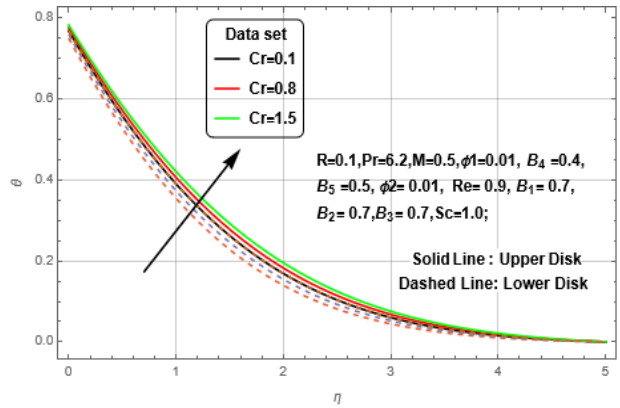

Figure 12. θ(η) vs η effect of Cr

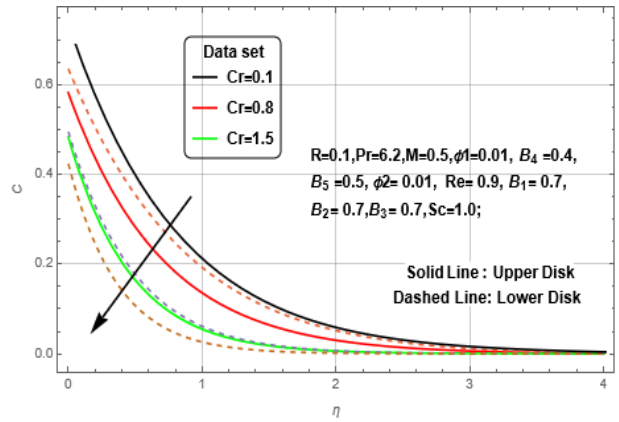

Figure 13. C(η) vs η effect of Cr

The error histogram (Figure 16) indicates that most prediction errors are concentrated at the value zero, with the training, validation, and test subsets exhibiting similar distributions. This means that there is a steady performance on data splits and a low bias. Lastly, Figure 17 shows regression plots with correlation coefficients (R-values) for each subset: training (R = 0.34336), validation (R = 0.53572), test (R = 0.45701), and overall (R = 0.41044). Although the R-values are moderate in terms of correlation, the fact that the slope and the intercept are always the same in subsets indicates that the model can extract underlying data trends [22-26]. All these numbers confirm that the LM-ANN surrogate model is highly tuned to predict the heat and mass transfer measures in the Aloe vera-ZnO/water hybrid nanofluid system, providing reliable parametric information at a low computational cost.

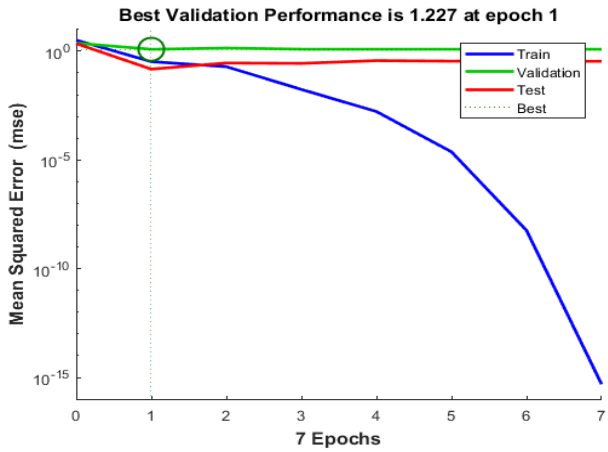

Figure 14. Best validation performance

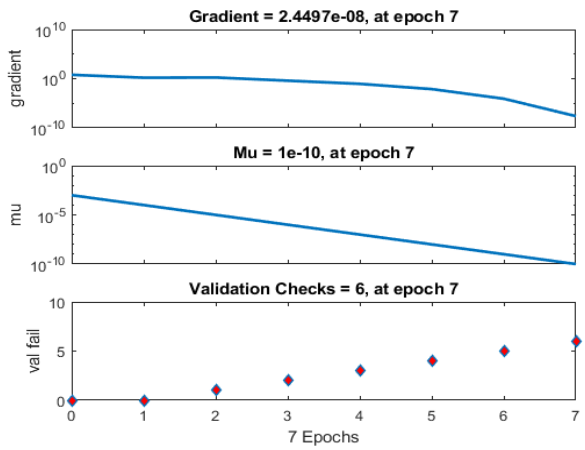

Figure 15. Gradient, Mu, validation

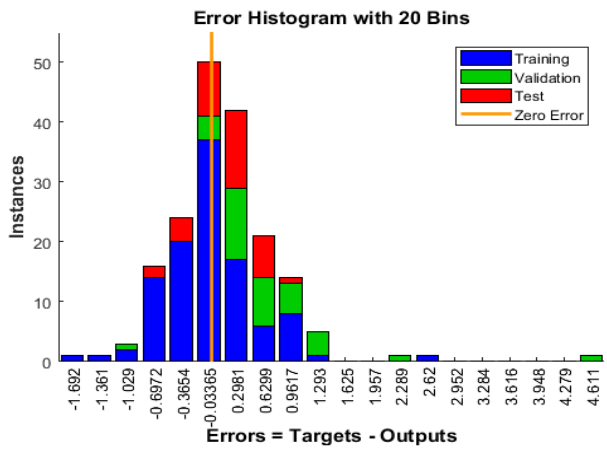

Figure 16. Error histogram

Table 2. The numerical values of the skin friction coefficient, Nusselt number for upper and lower disks of ternary nanofluid over a double disk

ϕ1	ϕ2	M	R	Sc	Cr	Cfx-Upper Disk-Aloe Vera–ZnO/Water Hybrid Nanofluid	Cfx-Lower Disk-Aloe Vera–ZnO/Water Hybrid Nanofluid	Nux-Upper Disk-Aloe Vera–ZnO/Water Hybrid Nanofluid	Nux-Lower Disk-Aloe Vera–ZnO/Water Hybrid Nanofluid
0.01	.01	0.5	0.1	1.0	0.1	0.73168	0.71243	0.57952	0.53444
0.02	0.01	0.5	0.1	1.0	0.1	0.77993	0.76145	0.55325	0.52209
0.03	0.01	0.5	0.1	1.0	0.1	0.81727	0.79172	0.51997	0.50143
0.01	0.02	0.5	0.1	1.0	0.1	0.58336	0.56248	0.50064	0.49992
0.01	0.05	0.5	0.1	1.0	0.1	0.51128	0.48720	0.49330	0.47915
0.01	0.08	0.5	0.1	1.0	0.1	0.46743	0.43242	0.48774	0.45850
0.01	0.01	0.5	0.1	1.0	0.1	0.79079	0.67566	0.49893	0.53442
0.01	0.01	1.0	0.1	1.0	0.1	0.98067	0.89111	0.46115	0.52349
0.01	0.01	1.5	0.1	1.0	0.1	1.13714	1.06210	0.41988	0.50978
0.01	0.01	0.5	0.4	1.0	0.1	0.79247	0.46309	0.48979	0.54423
0.01	0.01	0.5	0.8	1.0	0.1	0.96398	0.39966	0.43405	0.51315
0.01	0.01	0.5	1.2	1.0	0.1	1.13019	0.36553	0.39007	0.49780
0.01	0.01	0.5	0.1	2.0	0.1	0.41236	0.37814	1.86542	1.74208
0.01	0.01	0.5	0.1	4.0	0.1	0.40128	0.36295	1.79467	1.65533
0.01	0.01	0.5	0.1	6.0	0.1	0.38972	0.34781	1.72351	1.56984
0.01	0.01	0.5	0.1	1.0	0.1	0.39845	0.36492	1.82367	1.69852
0.01	0.01	0.5	0.1	1.0	0.8	0.38673	0.34987	1.75206	1.61134
0.01	0.01	0.5	0.1	1.0	1.5	0.37428	0.33476	1.68149	1.52572

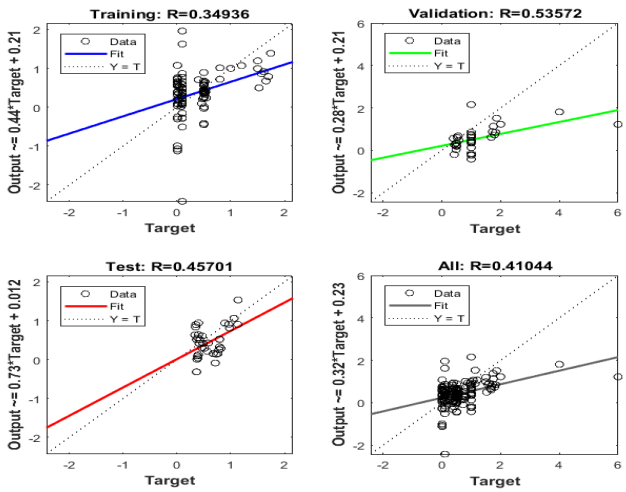

Figure17. Training, validation, test, All-R values

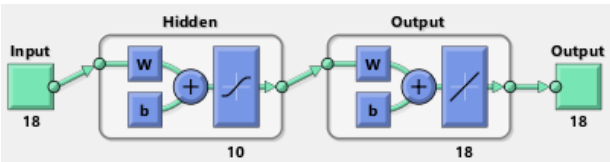

Figure 18. Neural network diagram

5. CONCLUSIONS

The following conclusions are drawn from the current study,

1. Raising the volume fraction of primary nanoparticles (ϕ_1), the magnetic parameter (M), and the Schmidt number (Sc) improves mass transfer properties, indicated by elevated Sherwood numbers and a reduced concentration boundary layer. This improvement is linked to increased diffusion and more pronounced concentration gradients in proximity to the disk surfaces. Nevertheless, this pattern is not consistent, as overly strong magnetic forces or excessively high Schmidt numbers can hinder flow and restrict additional enhancements in mass transfer.
2. Higher values of the radiation parameter (R), chemical reaction parameter (Cr), and secondary nanoparticle volume fraction (ϕ_2) typically result in lower thermal transport performance, which lowers the Nusselt number and attenuates velocity and concentration profiles across the flow domain.
3. Aloe vera/ZnO/water hybrid nanofluid provides environmentally friendly thermal improvement, which can be applied in rotating machines and bioreactors.
4. LM-trained ANN can predict the FEM results with high accuracy, with $R^2 > 0.98$.
5. The LM-trained ANN framework effectively substitutes the requirement for repetitive FEM computations, thereby enabling real-time prediction, optimization, and control in hybrid nanofluid engineering systems.
6. The present framework can form a paradigm as a digital twin basis for monitoring and controlling industrial heat transfer systems, particularly where rapid parametric assessment is needed for decision-making.
7. Future work could advance this method by incorporating additional hybrid nanoparticles, non-Newtonian base fluids, or transient effects to generalize the predictive capability of the AI model across diverse physical domains.

REFERENCES

[1] Afzal, S., Ullah, K., Shafique, M., Alamri, S.Z., Tlili, I. (2023). Heat and mass transfer with entropy optimization in hybrid nanofluid flow between rotating disks. Scientific Reports, 13: 11862. https://doi.org/10.1038/s41598-023-39176-5

[2] Noreen, S., Farooq, U., Waqas, H., Fatima, N., Alqurashi, M.S., Imran, M., Akgül, A., Bariq, A. (2023). Comparative study of ternary hybrid nanofluids with role of thermal radiation and Cattaneo-Christov heat flux between double rotating disks. Scientific Reports, 13:

7795. https://doi.org/10.1038/s41598-023-34783-8
[3] Yahaya, R.I., Arifin, N.M., Pop, I., Ali, F.M., Isa, S.S.P.M. (2024). Hybrid nanofluid flow over a shrinking rotating disk. Fluids, 12(7): 141. https://doi.org/10.3390/computation12070141
[4] Nasir, S., Berrouk, A.S., Gul, T., Ali, A. (2023). Develop the artificial neural network approach to predict heat transport in hybrid (Ag + MgO)/water nanofluid flow and energy transport in a magnetized porous cavity. Scientific Reports, 13: 21039. https://doi.org/10.1038/s41598-023-48412-x
[5] Ramzan, M., Shahmir, N., Ghazwani, H.A.S., Nisar, K.S., Alharbi, F.M., Yahia, I.S. (2022). Hybrid nanofluid flow induced by an oscillating disk. Scientific Reports, 12: 436. https://doi.org/10.1038/s41598-021-04173-z
[6] Alqahtani, A.M., Bilal, M., Ali, A., Alsenani, T.R., Eldin, S.M. (2023). Numerical solution of an electrically conducting spinning flow of hybrid nanofluid comprised of silver and gold nanoparticles across two parallel surfaces. Scientific Reports, 13: 7180. https://doi.org/10.1038/s41598-023-33520-5
[7] Sakkaravarthi, K., Bala Anki Reddy, P., Sakthi, I. (2024). Entropy optimization in Casson tetra-hybrid nanofluid flow over a rotating disk with nonlinear thermal radiation: A Levenberg–Marquardt neural network approach. Journal of Computational Design and Engineering, 11(5): 333-354. https://doi.org/10.1093/jcde/qwae086
[8] Kotike, J., Beedalannagari, O., Rekapalli, L., Usman, M., Kadavakollu, K.R. (2025). Neural network modeling of CuO/Au hybrid nanofluid thermal performance with slip effects for advanced process applications. Processes, 13(2): 516. https://doi.org/10.3390/pr13020516
[9] Mahariq, I., Ullah, K., Fiza, M., Jan, A.U., Ullah, H., Islam, S., Al-Mekhlafi, S.M. (2025). Levenberg–Marquardt recurrent neural network for heat transfer in ternary hybrid nanofluid flow with nonlinear heat source-sink. Advances in Mechanical Engineering, 17(6). https://doi.org/10.1177/16878132251341968
[10] Kumar, A., Sharma, B.K., Almohsen, B., Pérez, L.M., Urbanowicz, K. (2025). Artificial neural network analysis of Jeffrey hybrid nanofluid with gyrotactic microorganisms for optimizing solar thermal collector efficiency. Scientific Reports, 15: 4729. https://doi.org/10.1038/s41598-025-88877-6
[11] Islam, T., Gama, S., Martins Afonso, M. (2025). Artificial neural network and response surface methodology-driven optimization of Cu–Al_2O_3/water hybrid nanofluid flow in a wavy enclosure with inclined periodic magnetohydrodynamic effects. Mathematics, 13(1): 78. https://doi.org/10.3390/math13010078
[12] Mehmood, R., Ali, H.M. (2022). Thermophysical characterization of Aloe vera-based bio-nanofluids with ZnO nanoparticles for sustainable thermal applications. Case Studies in Thermal Engineering, 31: 101812. https://doi.org/10.1016/j.csite.2022.101812
[13] Ali, H. M., Babar, H., Shah, T.R., Qasim, M.A., Javed, S., Ali, A. (2020). Preparation techniques of bio-based nanofluids and their potential role in thermal applications: A review. Journal of Molecular Liquids, 297: 111919. https://doi.org/10.1016/j.molliq.2019.111919
[14] Sundar, L.S., Singh, M.K., Sousa, A.C.M., Chang, S.W. (2017). Investigations in heat transfer and friction factor of water-based Al_2O_3 and ZnO nanofluids in a tube with twisted tape inserts. International Journal of Heat and Mass Transfer, 100: 691-703. https://doi.org/10.1016/j.ijheatmasstransfer.2016.04.071
[15] Dasore, A., Konijeti, R., Prakash, B.O., Yelamasetti, B. (2024). Numerical and empirical simulation of fluid flow in a spiral plate heat exchanger with Nusselt number correlation development. International Journal on Interactive Design and Manufacturing, 18: 3103-3113. https://doi.org/10.1007/s12008-023-01454-x
[16] Redouane, F., Jamshed, W., Eid, M.R., Uma Devi, S.S., Musa, A., Eldin, S.M., Prakash, M., Ullah, I. (2022). Finite element methodology of hybridity nanofluid flowing in diverse wavy sides of penetrable cylindrical chamber under a parallel magnetic field with entropy generation analysis. Micromachines, 13(11): 1905. https://doi.org/10.3390/mi13111905
[17] Ali, B., Naqvi, R.A., Haider, A., Hussain, D., Hussain, S. (2020). Finite element study of MHD impacts on the rotating flow of Casson nanofluid with the double diffusion Cattaneo-Christov heat flux model. Mathematics, 8(9): 1555. https://doi.org/10.3390/math8091555
[18] Nadeem, S., ur Rehman, A., Hamed, Y.S., Riaz, M.B., Ullah, I., Alzabut, J. (2024). Finite-element method for natural convection flow of Casson hybrid nanofluid (Al_2O_3–Cu/water) inside H-shaped cavity. AIP Advances, 14: 085130. https://doi.org/10.1063/5.0218934
[19] Rashid, A., Ayaz, M., Islam, S. (2023). Mixed convection MHD hybrid nanofluid flow between two parallel rotating disks with Joule heating and chemical reactions. Mathematics and Mechanics of Solids, 28(1): 142-164. https://doi.org/10.1177/16878132231179611
[20] Tejes, P.K.S., Naik, B.K., Dasore, A., Hashim, N. (2025). Multi-objective optimization of a three-fluid hollow fiber membrane dehumidifier for energy-efficient drying applications. Case Studies in Thermal Engineering, 75: 107036. https://doi.org/10.1016/j.csite.2025.107036
[21] Kotnurkar, A., Gowda, S. (2024). Influence of magnetic field and activation energy on creeping flow of tri-hybrid nanofluid driven by peristaltic pumping in an asymmetric channel with synthetic cilia. Discover Mechanical Engineering, 3: 38. https://doi.org/10.1007/s44245-024-00074-3
[22] Vishalkumar, V., Prajapati, J., Meher, R.R. (2025). Analysing Soret, Dufour, and activation energy effects on heat and mass transfer thin film flow of an MHD Williamson ternary hybrid nanofluid over a non-Darcy porous stretching surface. The European Physical Journal Plus, 140: 672. https://doi.org/10.1140/epjp/s13360-025-06103-8
[23] Anand, N., Uppalapati, S., Padamurthy, A., Kishore Kumar, P., Kumar, G.N., Vemanaboina, H. (2025). Building enhanced neural network models to predict energy storage density of composite materials for low-temperature thermochemical energy storage. Journal of Energy Resources Technology, Part A: Sustainable and Renewable Energy, 1(6): 062501. https://doi.org/10.1115/1.4069225
[24] Uppalapati, S., Paramasivam, P., Kilari, N., Chohan, J.S., Kanti, P.K., Vemanaboina, H., Dabelo, L.H., Gupta, R. (2025). Precision biochar yield forecasting employing random forest and XGBoost with Taylor diagram visualization. Scientific Reports, 15(1): 7105. https://doi.org/10.1038/s41598-025-91450-w
[25] MM, V., Uppalapati, S., Battula, A., Kasturi, S.B.,

Vemanaboina, H., Kumar, S. (2025). Virtual prediction of residual stresses in laser welding process using machine learning technique an industry 4.0 approach. Journal Européen des Systèmes Automatisés, 58(5): 983-990. https://doi.org/10.18280/jesa.580512

[26] Gayatry, B., Shivaram Reddy, K., Haripriya, T., Ravi Kumar, Y., Vemanaboina, H., Veera Raghavulu, K. (2025). Prediction of residual stresses and distortion in GTA welding process using machine learning techniques. Applications of AI in Smart Technologies and Manufacturing, CRC Press, 66-72. https://doi.org/10.1201/9781003602453-8

[27] Konijeti, R., Dasore, A., Rajak, U., Kumar, R., Sharma, A., Yadav, A.S. (2024). CFD analysis of heat transfer by free convection over a vertical cylinder with circular fins of triangular cross-section. Multiscale and Multidisciplinary Modeling, Experiments and Design, 7: 741-753. https://doi.org/10.1007/s41939-023-00237-x